Indirect Evidence for the Supersymmetric Nature of Dark Matter from the Combined Data on Galactic Positrons, Antiprotons and Gamma Rays

> W. de Boer, M. Herold, C. Sander, V. Zhukov Institut für Experimentelle Kernphysik, Universität Karlsruhe (TH),
> P.O. Box 6980, 76128 Karlsruhe, Germany

> > September 26, 2021

Abstract

Two new observations have strengthened the case for the supersymmetric nature of the Cold Dark Matter component in our universe: First, it was shown that new data on the nuclear abundance, B/C - and ¹⁰Be/⁹Be ratios constrain the diffusion parameters in Galactic Models so strongly, that they lead to a clear deficiency in the production of diffuse hard gamma rays, antiprotons and hard positrons, if no anomalous sources or anomalous energy dependence of the diffusion coefficients are postulated. Second, from the precise relic density measurement by WMAP the WIMP annihilation cross section can be determined in a model independent way. If the WIMPS are postulated to be the neutralinos of Supersymmetry, then only a limited region of parameter space matches this annihilation cross section. It is shown that the resulting positrons, antiprotons and gamma rays from the neutralino annihilation (mainly into $b\bar{b}$ quark pairs) provide the correct shape and order of magnitude for the missing fluxes in the Galactic Models. Here the shape is the most discriminating feature, since for relatively heavy neutralinos the positron and gamma spectra from neutralino annihilation are significantly harder than the spectra produced by secondary interactions. For the antiprotons the shapes of background and signal are similar, but they still provide a strong constraint by the requirement of not overproducing antiprotons. The fitted normalization factors for antiprotons, positrons and gammas from neutralino annihilation come all out to be similar and below 10 for a standard NRW halo profile. It should be pointed out, that it is absolutely non-trivial to solve all three deficiencies simultaneously with a common halo profile, because the mean free paths of photons, antiprotons and positrons are quite different, so the observed fluxes come from different regions of the galaxy. The probability of a global fit to the galactic spectra of diffuse gamma rays, positrons and antiprotons improves from about 10^{-8} to 0.5, if Dark Matter. as predicted by Supersymmetry, is taken into account. This corresponds to about 6σ evidence for the supersymmetric nature of Dark Matter in case of Gaussian errors.

1 Introduction

Cold Dark Matter (CDM) makes up 23% of the energy of the universe, as deduced from the temperature anisotropies in the Cosmic Microwave Background (CMB) in combination with data on the Hubble expansion and the density fluctuations in the universe [1]-[4]. The nature of the CDM is unknown, but one of the most popular explanation for it is the neutralino, a stable neutral particle predicted by Supersymmetry [5, 6]. The neutralinos are spin 1/2 Majorana particles, which can annihilate into pairs of Standard Model (SM) particles. The stable decay and fragmentation products are neutrinos, photons, protons, antiprotons, electrons and positrons. From these, the protons and electrons are drown in the many matter particles in the universe, but the others may be detectable above the background from nuclear interactions, especially because of the much harder spectra expected from neutralino annihilation. The background is strongly constrained by the recent, precise

measurements of the fluxes of all nuclei in the galaxy, especially the ratios of secondary/primary nuclei and radioactive/non-radioactive isotopes. The diffusion and reacceleration parameters deduced from these data describe the fluxes of all matter particles in the galaxy, but they predict too few antiprotons, hard gammas, and positrons [7, 8]. Several ad hoc proposals have been made to solve these deficiencies, like unphysical breaks in the diffusion coefficient or postulating "unprocessed" fresh components in a "Local Bubble", which is different from the rest of the galaxy [9], or in order to obtain more high energy gammas one has either to postulate a local hard nuclear component generating hard π_0 's or a local hard electron spectrum to create hard gammas by inverse compton scattering [8].

However, none of these proposals solves these deficiencies simultaneously. In this paper we consider the annihilation of Dark Matter particles as a source for the missing gamma rays, antiprotons and positrons. A statistical analysis of all three species simultaneously provides a rather stringent test, since the mean free path is quite different for gamma rays, antiprotons and positrons. If one can solve the deficiencies of all three simultaneously for a single halo density profile and a single set of SUSY parameters, then this can be considered as a 'smoking gun' signature for the supersymmetric nature of the Cold Dark Matter, at least if the statistical significance is sufficient. Fortunately, the recent improvement in the cosmic parameters severely constrains the background calculation, while the precise WMAP data on the relic density implies a precise and model-independent measurement of the annihilation cross section: a larger annihilation cross section would imply a lower relic density and vice versa. Such an annihilation cross section can only be obtained for rather restricted regions of the SUSY parameter space. It will be shown that these SUSY parameters combined with the best known Galactic Model improve the probability of the fit to the measured galactic fluxes of diffuse gamma rays, antiprotons and positrons by 8 orders of magnitude, which corresponds to more than 6σ evidence for the supersymmetric nature of Dark Matter in case of Gaussian errors.

Indirect detection of Dark Matter has been discussed much before [10]-[51]. Our results differ from these previous results by performing a statistical analysis to positrons, antiprotons and gamma rays simultaneously and taking into account the best known propagation models. Furthermore, previous results never considered the shape of the gamma spectrum, which turns out to be a discriminating feature of the present analysis, since for the relatively heavy neutralinos the diffuse gamma spectrum from π_0 decays is considerably harder than the spectrum from secondary interactions. Also most of the previous analysis were done before the WMAP data became available and before the new satellite data on nuclear fluxes constrained the galactic background processes.

We do not consider neutrino detection, since for neutrinos no precise data are available. We restrict us to neutralino annihilation in the Minimal Supersymetric Model (MSSM) with gravity inspired supersymmetry breaking and radiative electroweak symmetry breaking, since this simplest model already gives a good description of the considered fluxes. Actually all we need from the model is stable neutralinos in the mass range of a few 100 GeV, which annihilate predominantly into hadronic final states. The cross sections turn out to be correct for values of the ratio of neutral Higgs vacuum expectation values around 50, as expected in SO(10) type of models[52]. In this case the neutralino annihilation into b-quarks pairs via pseudoscalar Higgs exchange dominates and the neutralino is predominantly photino-like, or more popular, Dark Matter is the supersymmetric partner of the Cosmic Microwave Background (CMB).

In the following we first describe the model independent determination of the annihilation cross section from the relic density. In the next section the predictions from Supersymmetry concerning neutralino annihilation are discussed, while in the following section the deficiencies in the gamma rays, antiprotons and positrons, as predicted by the Galprop model [53, 54] are discussed. In the last section the global fits are discussed. They are performed within the frame work of the DarkSusy [55] program, after modifying it to obtain the background and propagation model from Galprop in DarkSusy in order to have consistent propagation and diffusion for antiprotons and positrons from the two sources: nuclear interactions and neutralino annihilation. For the SUSY particle spectrum we use Suspect [56], for the Higgs masses Feynhiggsfast [57] and as a cross check for the cross sections and relic density we use Micromegas [58]. Finally, some expectations for direct detection and indirect searches for Dark Matter from solar neutrinos will be given.

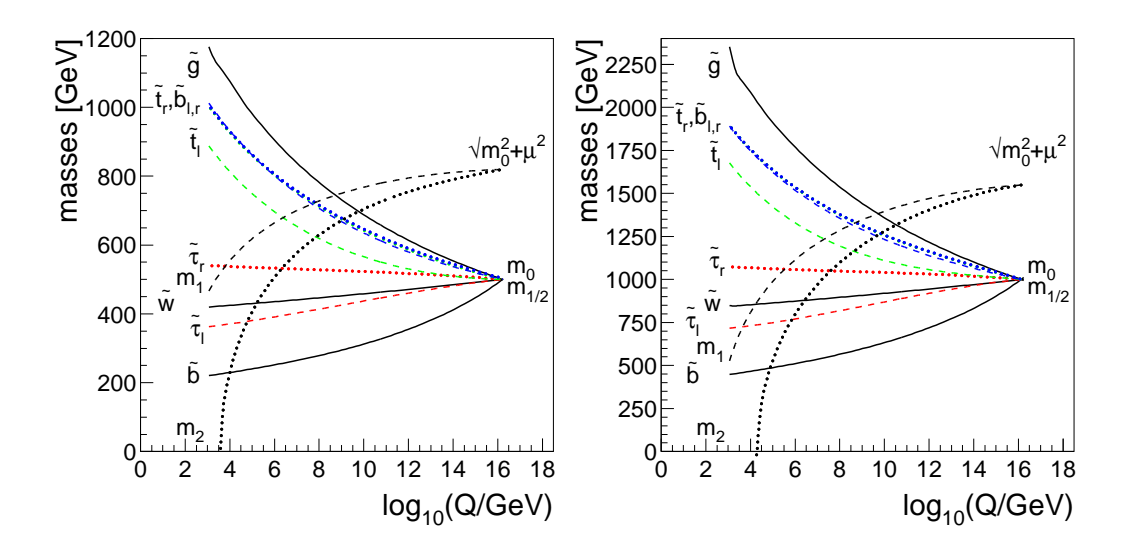


Figure 1: The running of the squark - and slepton masses starting at m_0 , gaugino masses starting at $m_{1/2}$ and Higgs mass parameters starting at $\sqrt{m_0^2 + \mu^2}$ for $m_0 = m_{1/2} = 500$ GeV and $\tan \beta = 51$ (left) and for $m_0 = m_{1/2} = 1000$ GeV and $\tan \beta = 53$ (right), which are the parameters of interest for the present analysis.

2 Annihilation Cross section Constraints from WMAP

In the early universe all particles were produced abundantly and were in thermal equilibrium through annihilation and production processes. The time evolution of the number density of the particles is given by the Boltzmann equation, which can be written for neutralinos as:

$$\frac{dn_{\chi}}{dt} + 3Hn_{\chi} = -\langle \sigma v \rangle (n_{\chi}^2 - n_{\chi}^{eq2}),\tag{1}$$

where H is the Hubble expansion rate, n_{χ} is the actual number density, n_{χ}^{eq} is the thermal equilibrium number density (before freeze-out), $<\sigma v>$ is thermally averaged value of the total annihilation cross section times the relative velocity of the annihilating neutralinos. The Hubble term takes care

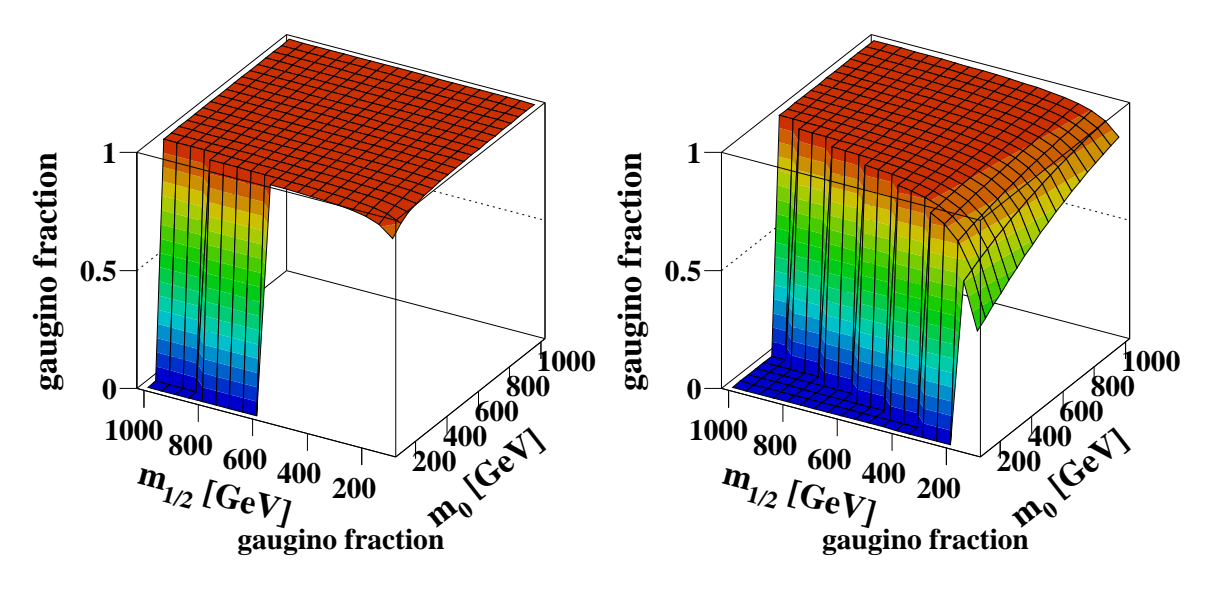


Figure 2: The gaugino fraction of the lightest neutralino as function of m_0 and $m_{1/2}$ for $\tan \beta = 10$ (left) and $\tan \beta = 50$ (right).

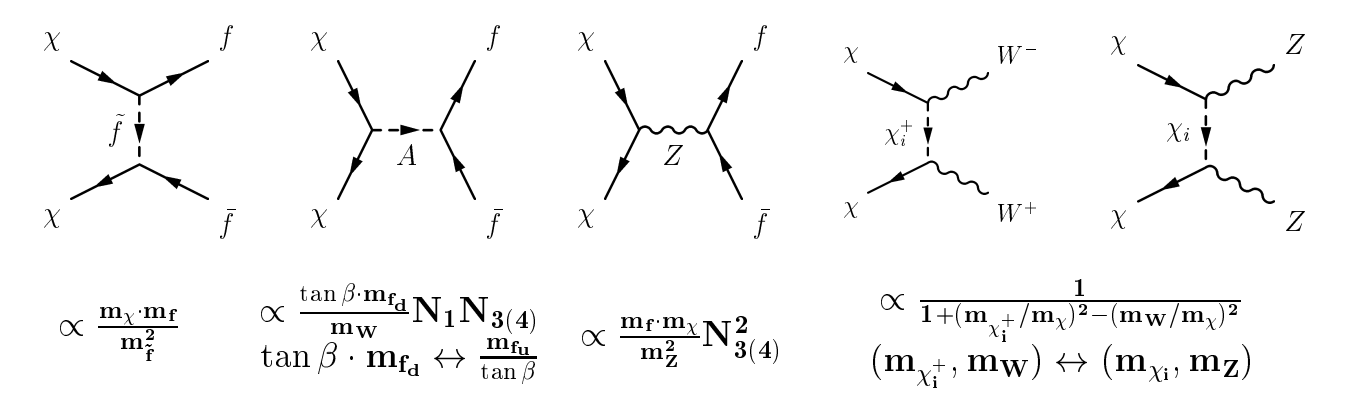


Figure 3: Dominant tree diagrams for Dark Matter annihilation. Note that the amplitudes of the graphs shown at the top are proportional to the mass of the final state fermion, while the Higgs exchange is proportional to $\tan \beta$ for d-type quarks and $1/\tan \beta$ for up-type quarks. This implies that light fermion final states can be neglected and at large $\tan \beta$ the bottom final states dominate.

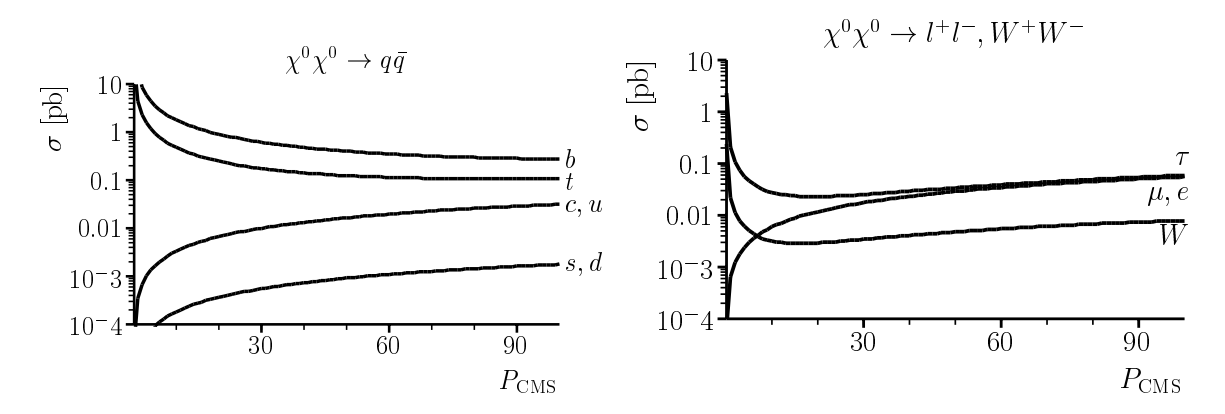


Figure 4: The neutralino annihilation total cross section for $\tan \beta = 35$ as function of the center of mass momenta in GeV of the neutralinos for quark -, lepton - and W^+W^- final states, as calculated with CalcHEP [61]. Note the helicity suppression at low momenta for light fermions.

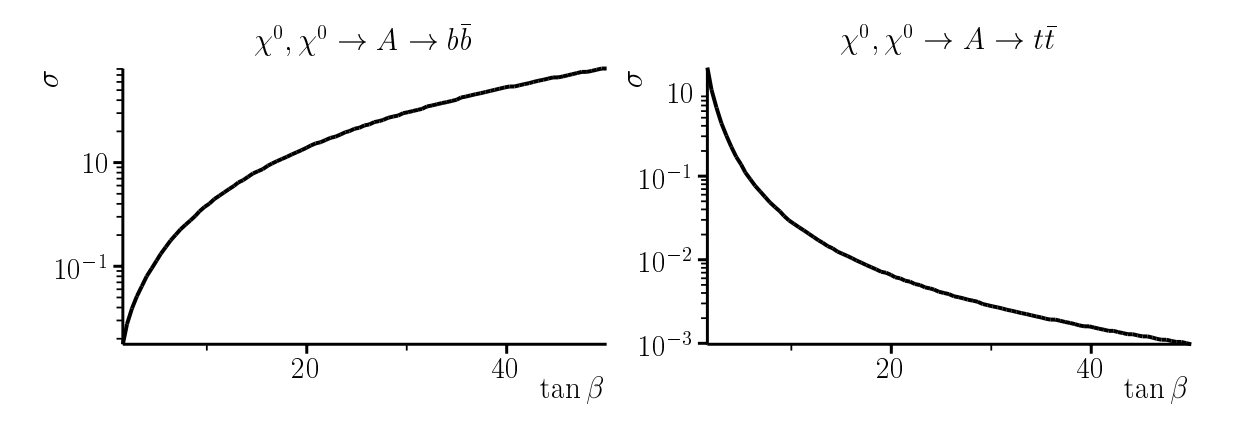


Figure 5: The neutralino annihilation cross section for pseudoscalar Higgs exchange for bottom and top final states as function of $\tan \beta$, as calculated with CalcHEP [61].

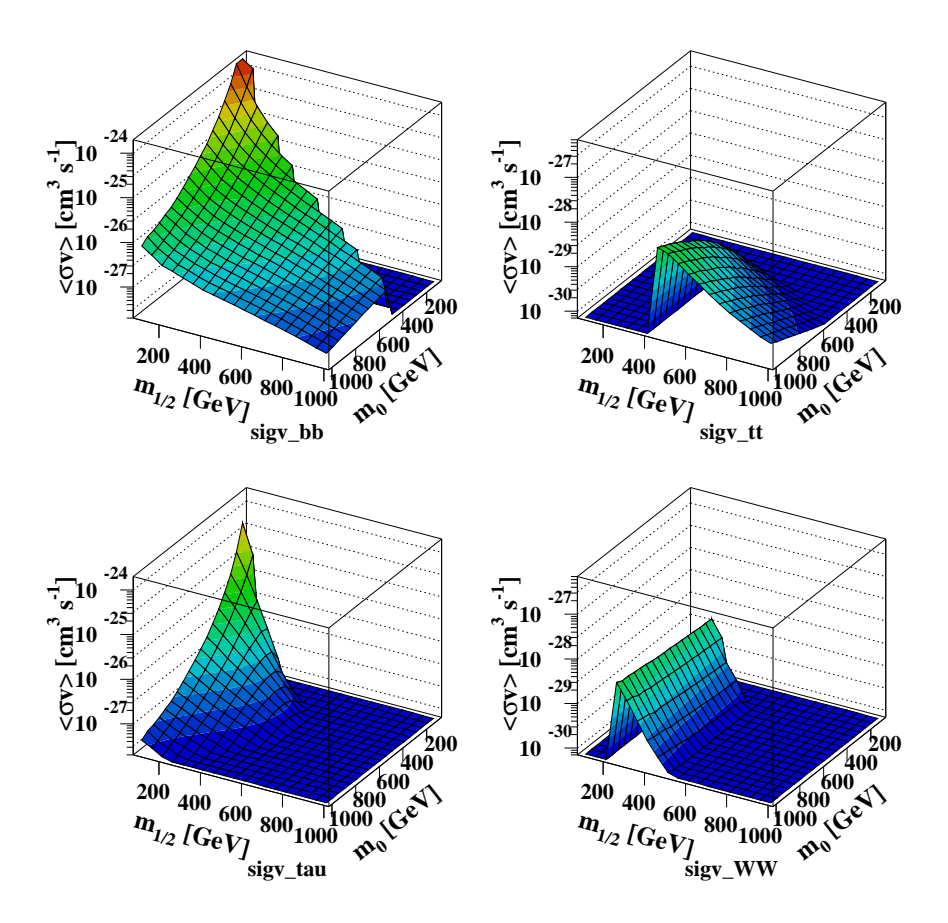


Figure 6: The thermally averaged annihilation cross section times velocity for neutralino annihilation as function of m_0 and $m_{1/2}$ for $\tan \beta = 50$ and $b\bar{b}$, $t\bar{t}$, W^+W^- , and $\tau\bar{\tau}$ final states (clockwise from top left). The results were calculated with DarkSusy [55].

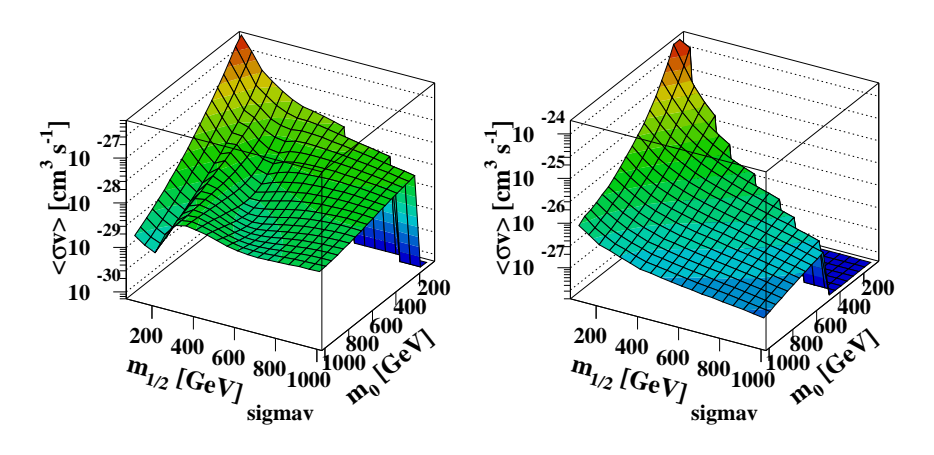


Figure 7: The thermally averaged total annihilation cross section times velocity for neutralino annihilation as function of m_0 and $m_{1/2}$ for $\tan \beta = 5$ (left) and 50 (right).) The neutralino mass equals $\approx 0.4 m_{1/2}$ in the CMSSM, so in the plots the neutralino varies from 40 to 400 GeV along the front axis. Note the strong decrease of the cross section for heavier SUSY mass scales and the different vertical scales due to the strong increase of the cross section with $\tan \beta$.

of the decrease in number density because of the expansion, while the first term on the right hand side represents the decrease due to annihilation and the second term represents the increase through creation by the inverse reactions.

At temperatures below the mass of the neutralinos the number density drops exponentially. The annihilation rate $\Gamma = \langle \sigma v \rangle n_{\chi}$ drops exponentially as well, and if it drops below the expansion rate, the neutralinos cease to annihilate. They fall out of equilibrium (freeze-out) at a temperature of about $m_{\chi}/25$ [37] and a relic cosmic abundance remains.

For the case that $\langle \sigma v \rangle$ is energy independent, which is a good approximation in case there is no coannihilation, the present mass density in units of the critical density is given by [6]:

$$\Omega_{\chi}h^2 = \frac{m_{\chi}n_{\chi}}{\rho_c} \approx \left(\frac{3 \cdot 10^{-27} cm^3 s^{-1}}{\langle \sigma v \rangle}\right). \tag{2}$$

One observes that the present relic density is inversely proportional to the annihilation cross section at the time of freeze out, a result independent of the neutralino mass (except for logarithmic corrections). For the present value of $\Omega_{\chi}h^2=0.1$ the thermally averaged total cross section at the freeze-out temperature of $m_{\chi}/25$ must have been $3 \cdot 10^{-27} cm^3 s^{-1}$. This can be achieved only for restricted regions of parameter space in the MSSM, as will be discussed in the next section.

3 Dark Matter Predictions from Supersymmetry

Supersymmetry [52] presupposes a symmetry between fermions and bosons, which can be realized in nature only if one assumes each particle with spin j has a supersymmetric partner with spin |j-1/2|(|j-1/2|) for the Higgs bosons). This leads to a doubling of the particle spectrum. Unfortunately the supersymmetric particles or "sparticles" have not been observed so far, so the sparticle masses must be above the limits set by searches at present accelerators. Obviously SUSY cannot be an exact symmetry of nature; or else the supersymmetric partners would have the same mass as the normal particles. The mSUGRA model, i.e. the Minimal Supersymmetric Standard Model (MSSM) with supergravity inspired breaking terms, is characterized by only 5 parameters: m_0 , $m_{1/2}$, $\tan \beta$, $\mathrm{sign}(\mu)$, A_0 . Here m_0 and $m_{1/2}$ are the common masses for the gauginos and scalars at the GUT scale, which is determined by the unification of the gauge couplings. Gauge unification is still possible with the precisely measured couplings at LEP [59]. The ratio of the vacuum expectation values of the neutral components of the two Higgs doublets in Supersymmetry is called $\tan \beta$ and A_0 is the trilinear coupling at the GUT scale. We only consider the dominant trilinear couplings of the third generation of quarks and leptons and assume also A_0 to be unified at the GUT scale. The constraints on the supersymmetric parameters space are practically independent of A_0 due to a coincidence from the constraints from the $b \to X_s \gamma$ rate and the lower limit on the Higgs mass of 114 GeV [59]. The absolute value of the Higgs mixing parameter μ is determined by electroweak symmetry breaking, while its sign is taken to be positive, as preferred by the anomalous magnetic moment of the muon [59].

The GUT scale masses are connected to low energy masses by the Renormalization Group Equations (RGE), as shown in Fig. 1. The running masses of the gauginos at low energy obey the simple solutions of the RGE:

$$M_i(t) = \frac{\tilde{\alpha}_i(t)}{\tilde{\alpha}_i(0)} m_{1/2}.$$
 (3)

Numerically at the weak scale $(t = 2 \ln(M_{GUT}/M_Z) = 66)$ one finds (see fig. 1):

$$M_3(\tilde{g}) \approx 2.7 m_{1/2}, \tag{4}$$

$$M_2(M_Z) \approx 0.8m_{1/2},\tag{5}$$

$$M_1(M_Z) \approx 0.4 m_{1/2}.$$
 (6)

The gluinos obtain corrections from the strong coupling constant α_3 ; therefore they grow heavier than the gauginos of the $SU(2)_L \otimes U(1)_Y$ group. Since the Higgsinos and gauginos are all spin 1/2

particles and are equal in all other quantum nubers, the mass eigenstates are in general mixtures of them, which are called generically charginos (neutralinos) for the mixture of the supersymmetric partners of the charged (neutral) gauge bosons and charged (neutral) Higgs bosons. The Majorana neutralino and Dirac chargino fields can be written as:

$$\chi = \begin{pmatrix} \tilde{B} \\ \tilde{W}^3 \\ \tilde{H}_1^0 \\ \tilde{H}_2^0 \end{pmatrix}, \quad \psi = \begin{pmatrix} \tilde{W}^+ \\ \tilde{H}^+ \end{pmatrix},$$

while the mass matrices can be written as [52]:

$$M^{(0)} = \begin{pmatrix} M_1 & 0 & -M_Z \cos \beta \sin \theta_W & M_Z \sin \beta \sin \theta_W \\ 0 & M_2 & M_Z \cos \beta \cos \theta_W & -M_Z \sin \beta \cos \theta_W \\ -M_Z \cos \beta \sin \theta_W & M_Z \cos \beta \cos \theta_W & 0 & -\mu \\ M_Z \sin \beta \sin \theta_W & -M_Z \sin \beta \cos \theta_W & -\mu & 0 \end{pmatrix}$$
(7)

$$M^{(c)} = \begin{pmatrix} M_2 & \sqrt{2}M_W \sin \beta \\ \sqrt{2}M_W \cos \beta & \mu \end{pmatrix}$$
 (8)

The last matrix leads to two chargino eigenstates $\tilde{\chi}_{1,2}^{\pm}$. The dependence on the parameters at the GUT scale can be estimated by substituting for M_2 and μ their values at the weak scale: $M_1(M_Z) = 2M_2(M_Z) \approx 0.4m_{1/2}$ and $\mu(M_Z) \approx 0.63\mu(0)$.

From Fig. 1 it can be seen that the mass parameters in the Higgs potential, m_1 and m_2 , are driven negative, largely because of the large Yukawa couplings of the third generation of quarks and leptons. This leads to radiative electroweak symmetry breaking (EWSB), so the Higgs mechanism in Supersymmetry needs not to be introduced ad hoc, as in the Standard Model, but is caused by radiative corrections. The running is only strong enough for top masses between 140 and 200 GeV and if the starting value $\sqrt{\mu^2 + m_0^2}$ at the GUT scale is large enough, which in practice implies $\mu > M_2$. From the mass matrices 7 and 8 it is clear that for $M_{1,2} < \mu$ the lightest chargino is wino-like with a mass given by M_2 if the mixing is neglected and similarly the lightest neutralino is bino like with a mass given by $M_1 \approx 0.5 M_2$.

In practice, there is some mixing and the neutralino mass eigenstates are linear combinations of the weak eigenstates, i.e.

$$\chi_i^0 = N_1 |\tilde{B}> + N_2 |\tilde{W}_3> + N_3 |\tilde{H}_1^0> + N_4 |\tilde{H}_2^0>.$$

The gaugino fraction $N_1^2 + N_2^2$ is nevertheless close to one, especially if the diagonal elements are large compared with the off-diagonal elements proportional to M_Z . This is demonstrated in Fig. 2.

The interaction of the sparticles with normal matter is governed by a new multiplicative quantum number called R-parity, which is needed in order to prevent baryon- and lepton number violation. In GUT theories quarks, leptons and Higgses are all contained in the same supermultiplet, which allows couplings between quarks and leptons. Such transitions, which could lead to rapid proton decay, are not observed in nature. Therefore, the SM particles are assigned a positive R-parity and the supersymmetric partners have a negative one, which can be related to the known conserved quantum numbers of spin S, baryon number B and lepton number L by $R = (-1)^{3B+l+2S}$. Requiring R-parity conservation implies that at each vertex one needs two supersymmetric particles, from which it follows that:

- The rapid proton decays involving vertices with only one sparticle do not occur.
- Sparticles can be produced only in pairs, e.g. $\overline{p}p \to \tilde{q}\tilde{g}X$ or $e^+ + e^- \to \tilde{\mu}^+\tilde{\mu}^-$.

- The heavier sparticles can decay to lighter ones, like $\tilde{e} \to e\tilde{\gamma}$ or $\tilde{q} \to q\tilde{g}$, but the Lightest Supersymmetric Particle (LSP) is stable, since its decay into normal matter would change R-parity.
- The LSP has to be neutral to be a good candidate for Dark Matter.
- The interactions of particles and sparticles can be different. For example, the photon couples to electron-positron pairs, but the photino does not couple to electron-positron or selectron-spositron pairs, since in these cases the R-parity would change from -1 to +1.
- The LSP is weakly interacting with normal matter, since the final state has to contain the LSP again, so its interaction with quarks would only be elastic scattering by e.g. Z-, Higgs or squark exchange.

Consequently, the LSP is an ideal candidate for Dark Matter, since it has all the properties of a Weakly Interacting Massive Particle (WIMP), namely it is neutral, heavy and weakly interacting, so it will form galactic haloes.

The neutralinos can annihilate through the diagrams, shown in Fig. 3. The main features of the amplitudes have been indicated below the diagrams:

- The annihilation into fermion-antifermion pairs is proportional to the fermion mass in the limit v→0, which is the important case in the present universe at a temperature of a few Kelvin. This can be understood as follows: The neutralino is a Majorana particle, so it is its own antiparticle. In addition it has spin 1/2, thus obeying Fermi statistics, which implies it cannot have identical quantum numbers. Furthermore at low velocity it annihilates into an s-wave state, which implies the spins have to be antiparallel (just like for electrons in the hydrogen s-wave). Therefore also the spins in the final state have to be antiparallel, which leads to an amplitude proportional to the fermion mass to account for the required helicity flip[60]. Consequently heavy final states are enhanced at low momenta, as demonstrated in Fig. 4. Note that at higher momenta not only s-waves contribute and the helicity suppression disappears, so during the time of freeze-out all final states were produced. Note that these arguments are only valid for the diagrams with sfermion and Z-exchange. For the Higgs exchange the proportionality to the final state fermion mass arises from the Yukawa coupling. These cross sections were calculated with the program package CalcHep[61].
- The second important point concerns the $\tan \beta$ dependence: the diagram via pseudoscalar Higgs exchange is proportional to $\tan \beta$ for down-type quarks and $1/\tan \beta$ for up-type quarks. This implies that at large $\tan \beta$ ($\tan \beta > 5$) the b-quark final states are enhanced over t-quark final states, as shown in Fig. 5. The amplitudes of the Higgs exchange and the Z-exchange have an opposite sign. Since the top final states have a large amplitude for Z-exchange (amplitude \propto mass), they are additionally suppressed by the negative interference with the t-channel amplitudes. The cross sections for various final states are shown as function of $m_0, m_{1/2}$ in Fig. 6. The strong increase of the total annihilation cross section as function of $\tan \beta$ is demonstrated in Fig. 7 in the $m_0, m_{1/2}$ plane, which also shows the strong dependence on the SUSY masses: only low SUSY scales and large $\tan \beta$ lead to cross sections of the order of magnitude required by the WMAP data (Eq. 2).
- As shown in Fig. 3, the amplitude for pseudoscalar Higgs exchange is proportional to $N_1N_{3,4}$, i.e. it requires that the lightest neutralino has both bino- and Higgsino components, which implies that the diagonal elements in the mass matrix 7 should not be too large compared with the off-diagonal elements proportional to M_Z . So unless one tunes $\tan \beta$ and the SUSY masses such that one hits the resonance $(m_A \approx 2m_\chi)$, in which case very small Higgsino admixtures are enough, one needs relatively light neutralino masses.

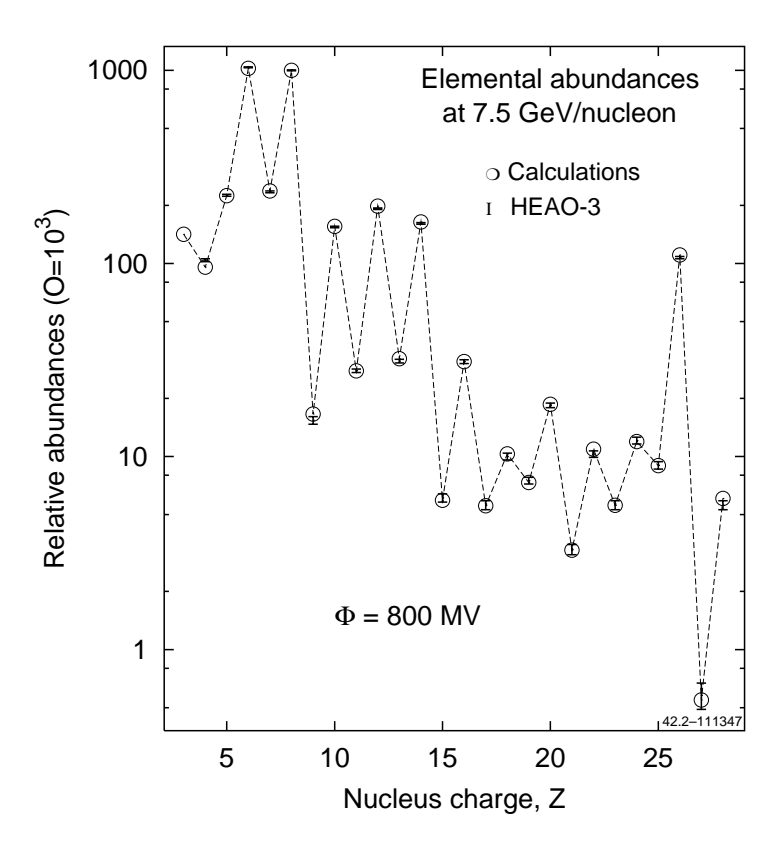


Figure 8: Propagated abundances at 7.5 GeV/nucleon, as calculated by Galprop in comparison with data. From Ref. [9].

In summary, the annihilation cross section becomes large for large $\tan \beta$ and is dominated for $\tan \beta > 5$ by the s-channel pseudoscalar Higgs exchange into $b\bar{b}$ quark pairs. Fig. 7 shows that values of $\tan \beta$ around 50 yield the annihilation cross sections required by WMAP, given in Eq. 2. Regions of coannihilation [62] at smaller $\tan \beta$ are allowed by WMAP data, but have too small annihilation cross sections to explain the deficiencies in the positron, antiproton and gamma ray fluxes, as will be shown in the last section. Before discussing the global fits, the cosmic ray fluxes from nuclear interactions are discussed.

4 Cosmic Rays generated by Nuclear Interactions

The sources of charged and neutral cosmic rays are believed to be supernovae and their remnants, pulsars, stellar winds and binary systems [53, 54]. Observations of X-ray and γ -ray emissions from these objects reveal the acceleration of charged particles near them. Particles accelerated near the sources propagate tens of millions of years in the interstellar medium where they can loose or gain energy and produce secondary particles and γ -rays. The spallation of primary nuclei into secondary nuclei gives rise to rare isotopes. Nuclear interactions produce not only matter, but also antimatter, like antiprotons and positrons. The latter originate mainly from the decay of charged pions and kaons.

The detailed studies of cosmic rays teach us about the production and propagation in the universe. The gammas can deliver information over intergalactic distances, while the charged particles propagate mainly on galactic distances. Secondary nuclei are produced in the galactic disc, from where they escape into the halo by diffusion and Galactic winds (convection). They may gain energy by "diffusive" reacceleration in the interstellar medium by the 2nd order Fermi acceleration mechanism, i.e. on average more interstellar gas clouds from opposite directions are hitting a given nuclei than "comoving" gas clouds. In elastic collisions this leads on average to an energy gain, thus depleting the low energy part of the source spectrum. Long-living radioactive secondaries tell how long they

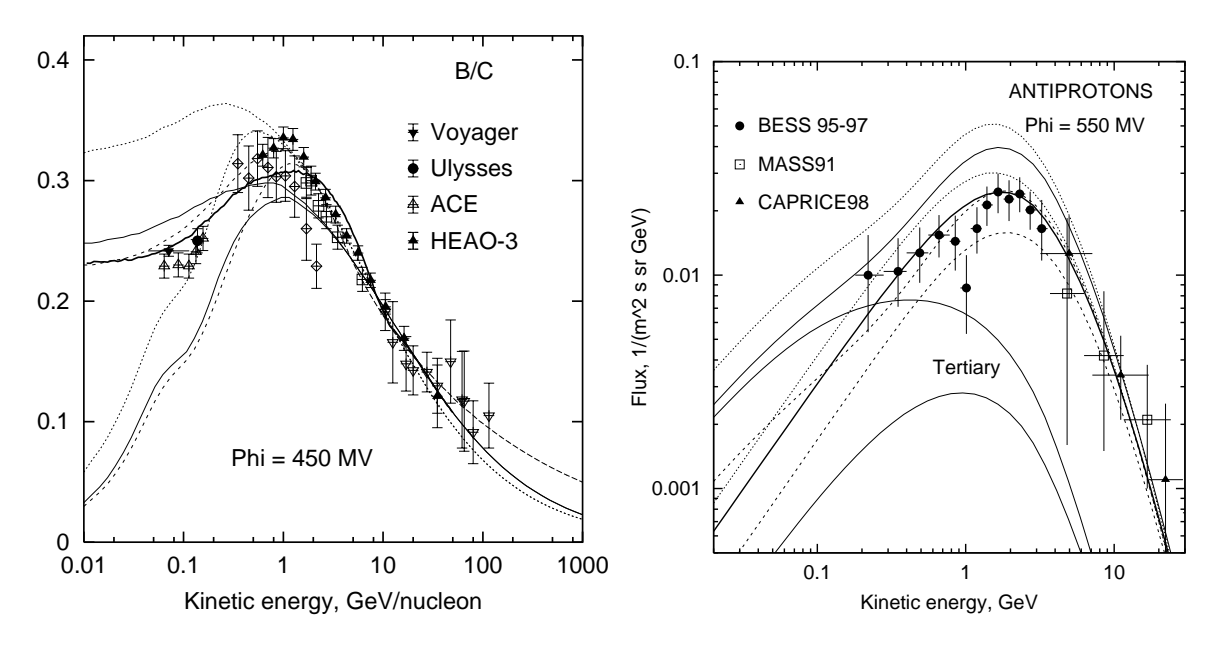


Figure 9: The B/C ratio as an example of secondary/primary nucleon ratios for various Galprop models in comparison with data. The dashed lines are the model with diffusive reacceleration, the solid ones for diffusion plus convection, and the dotted ones for plain diffusion. The lower (upper) curves of each kind are the interstellar (solar modulated) ones. The diffusive reacceleration curve (dashed) provides the best fit to the B/C ratio, but due to the large diffusion coefficient required, this leads to a deficiency in the flux of antiprotons (right). From Ref. [7].

survive in the halo before interacting in the disc again, thus determining the size of the halo. The gas density and acceleration time scale can be probed by the abundances of the K-capture isotopes, which would decay via electron K-capture in the interstellar gas.

A global fit to all this information allows one to build a model of our galaxy. Analytical and

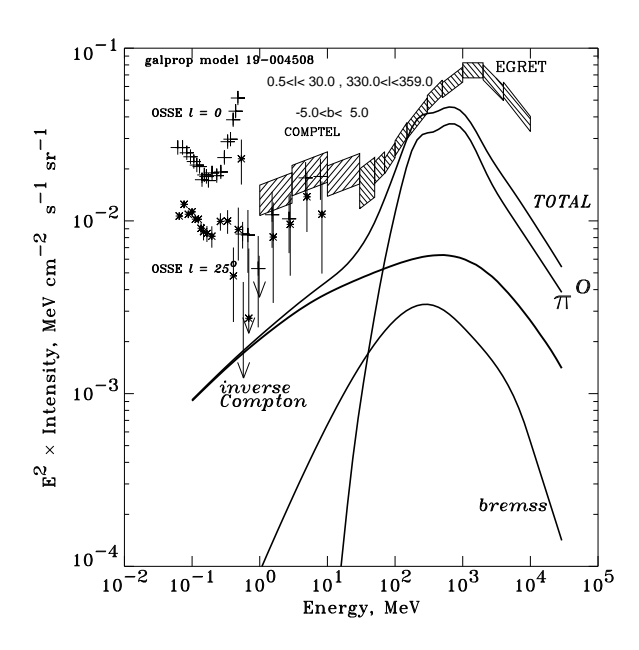


Figure 10: The gamma-ray energy spectrum of the inner Galaxy as calculated by Galprop [8] in comparison with EGRET data. Clearly, there is an access of data above 1 GeV.

semi-analytical models often fail when compared with all data. Therefore advanced models incorporating nuclear reaction networks, cross sections for production of antiprotons, positrons, γ -rays and synchrotron radiation, energy losses, convection, diffusive reacceleration, distribution of sources, gas and radiation field etc. are needed.

In addition, the distributions of matter and antimatter in the interstellar medium (ISM) are modified locally by affects of the solar activity and magnetic fields inside our solar system, e.g. from the planets. Gleeson & Axford [63] modelled the periodically varying solar activity with a typical half cycle of 11 years¹ by a radial solar wind in which the charged particles loose kinetic energy depending on their rigidity R and on the distance r from the sun. On this time scale the incoming flux from the Galaxy does not vary and the problem reduces to an adiabatical deceleration by the solar wind with a dependence only on the radial coordinate. This can be solved analytically:

$$J(r, E, t) = \frac{R^2}{R'^2} J(\inf, E'),$$
(9)

where J(r, E, t) is the measured differential flux at a distance r from the sun for particles with energy E and mass E_0^2/c^2 , $J(\inf, E')$ is the incoming flux to the solar system and $R^2 = (E^2 - E_0^2)/(Ze)^2$ is the rigidity with R' = R(E'). The energy loss can be parametrized by the solar modulation parameter $\Phi(t)$ as $E = E' - |Ze|\Phi(t)$, where |Ze| is the absolute charge of the particle; $\Phi(t)$ varies between 350 and 1500 MeV depending on the solar cycle. The solar modulation shifts the particle spectrum to lower energies, but the effect is only noticeable for rigidities below 10 GV. Recent determinations of the local interstellar flux (LIS) from the modulated (=measured) ones for electrons, positrons and protons can be found in Ref. [64].

The most complete and publicly available code for the production and propagation of particles in our galaxy is the Galprop code [53, 54]. It provides a numerical solution to the transport equation including a cross section database with more than 2000 points, source functions, density distributions, etc. The cross section tables include all possible cross sections: p+p, p+He, p+N, He+N, N+N, where all nuclei up to the heaviest ones (Ni) are considered. Fig. 8 shows the composition of the primary and secondary nuclei, as calculated by Galprop in comparison with data. Clearly, the production of secondary nuclei is well described.

Fig. 9 shows the spectrum of the Boron over Carbon (B/C) ratio, which shows a characteristic depletion at low energies. Since Boron is a purely secondary produced nuclei, while Carbon is primarily produced, the depletion at low energy is a sensitive handle on the question of diffusive reacceleration and solar modulation. As shown, the modulation effects the spectra mainly at kinetic energies below 10 GeV/nucleon. In order to reproduce the sharp peak in the ratios of secondary to primary nuclei without any unphysical breaks in the energy dependence of the diffusion coefficients and/or the injection spectrum, the diffuse reacceleration with a rather large diffusion coefficient is needed [7]. But this leads to too few antiprotons, as shown by the dashed line on the right hand side in Fig. 9. The possible way out of the discrepancy between the B/C ratio and too few antiprotons was suggested by Strong and Moskalenko: a "fresh" local unprocessed component at low energies of primary nuclei, thus decreasing the B/C ratio and allowing for a smaller diffusion coefficient. Also too few gammas are generated by Galprop, as shown in Fig. 10, which would also need either a harder nucleon spectrum or a harder electron spectrum, but this would need spatial variations which make the spectrum in our local region unrepresentative of the large scale average [8].

However, an alternative explanation may be the annihilation of neutralinos, which increases the yield of gammas, antiprotons, and high energy positrons, but does NOT effect the B/C ratio. This goes exactly in the direction of solving these discrepancies between Galprop and present data *simultaneously*, as will be shown in the next section by a global fit to all data.

¹A cycle can vary between 8 and 14 yr.

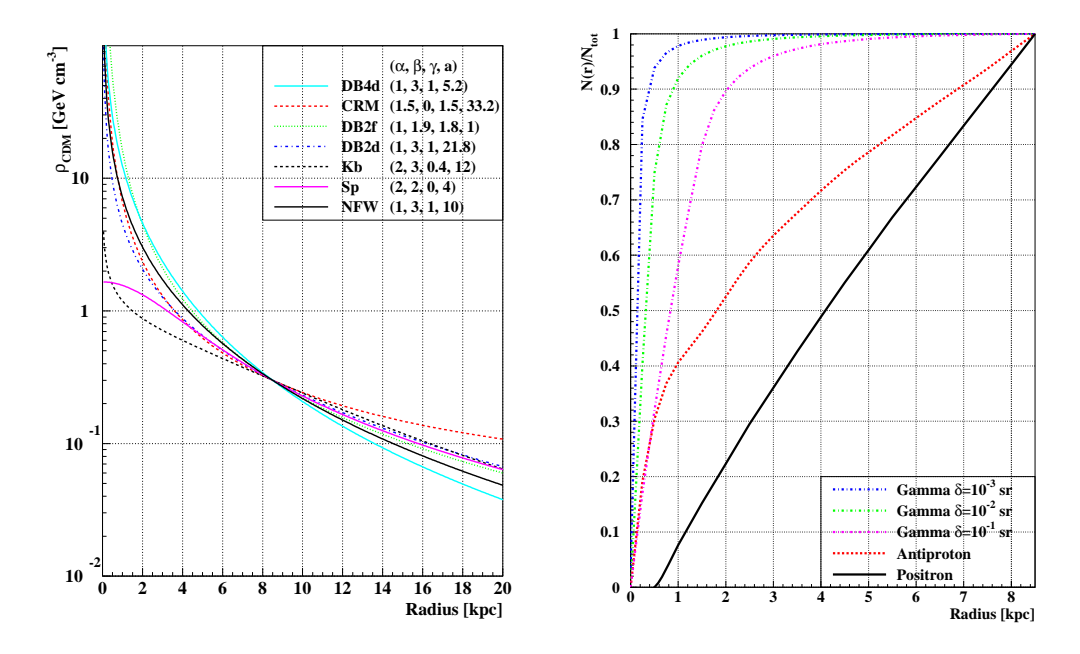


Figure 11: The halomodel used in this paper in comparison with other halomodels in the literature (left) and the integrated fraction of the fluxes as function of the distance from the center of the galaxy (right). One observes that more than 50% of the gamma rays originate from a region of less than 0.2 (1.5) kpc from the center for a detector subtending a solid angle of 10^{-3} (10^{-1}) sr, while the antiprotons and positrons reach the 50% at 1.9 and 4.1 kpc, respectively.

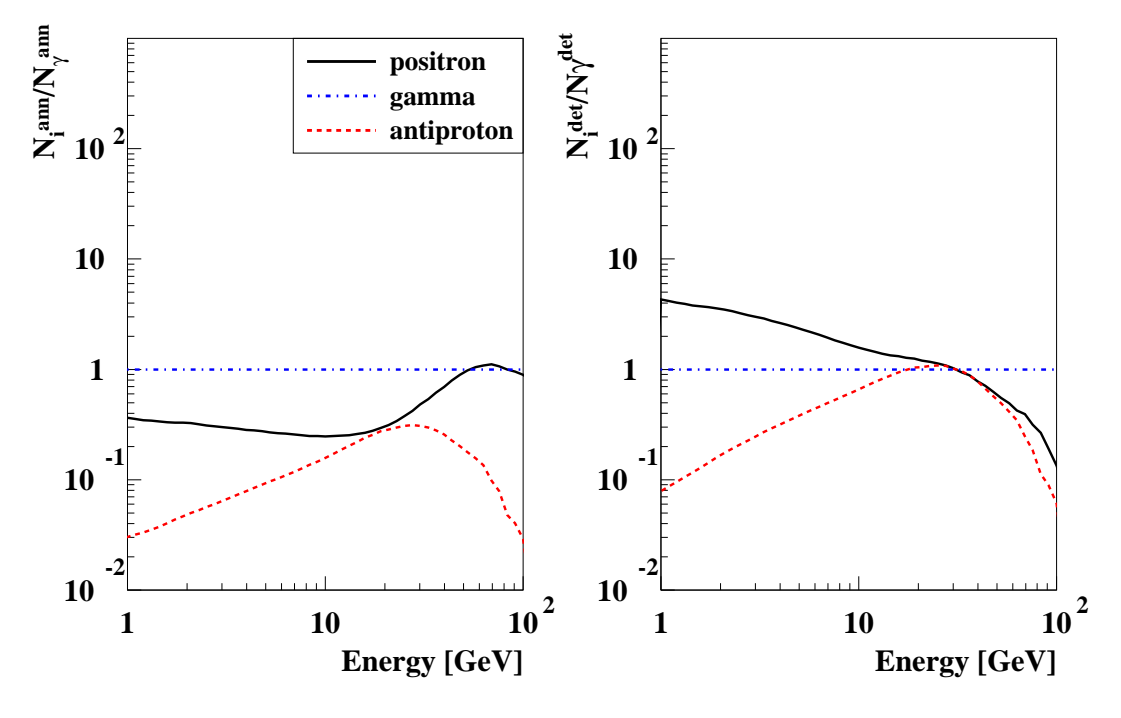


Figure 12: The flux of antiprotons and positrons normalized to the gamma flux from neutralino annihilation before (left) and after (right) diffusion with the halomodel and diffusion parameters described in the text.

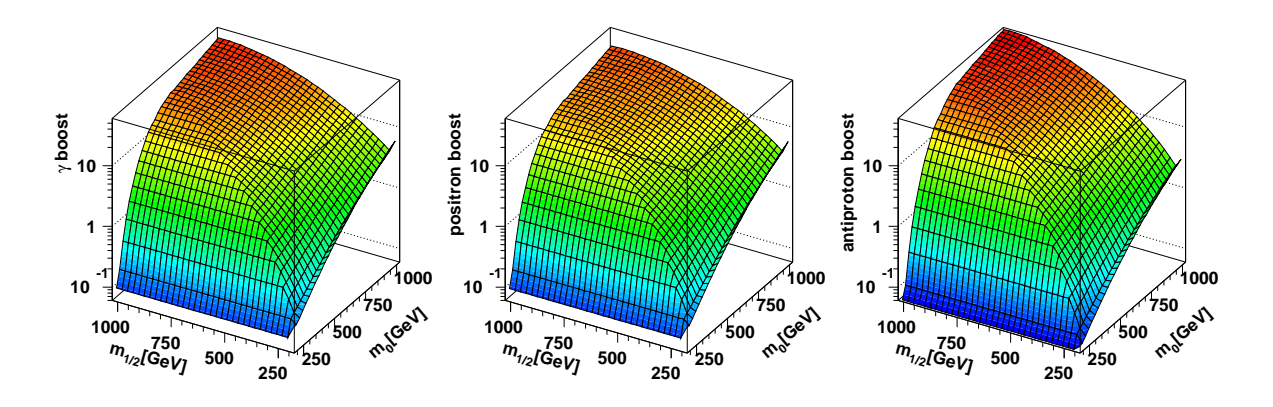


Figure 13: Boost factors for gamma rays, positrons and antiprotons (from left to right) as function of m_0 and $m_{1/2}$ for $\tan \beta = 51$. Note that the boost factors are similar for all three fluxes, which is a strong constraint for any model.

5 Global Fits to positrons, antiprotons and gamma rays

Trying to disentangle the contributions from nuclear interactions and neutralino annihilation to the antimatter fluxes and gamma rays is in practice not easy. Ideally one would like to implement the neutralino annihilation as a source function in the Galprop code, so the antimatter and gamma rays from nuclear interactions and annihilation would be transported through the galaxy in an identical way. However, this numerical code is too slow to be used in a fit program. Therefore, we used the second best possibility, namely using the publicly available code DarkSusy [55] for neutralino annihilation, which has semi-analytical solutions to the diffusion equation and includes the important energy losses for positrons. We changed the diffusion parameters and code in DarkSusy in such a way, that the results resembled as closely as possible the Galprop results. The main difference in the diffusion parameters between DarkSusy and Galprop lies in the fact that Galprop uses diffusive reacceleration, while DarkSusy does not. The diffusive reacceleration is needed to fit the B/C ratio and results in an almost order of magnitude larger diffusion constant with a much smaller energy dependence. The diffusion parameters and energy losses in DarkSusy were changed as follows:

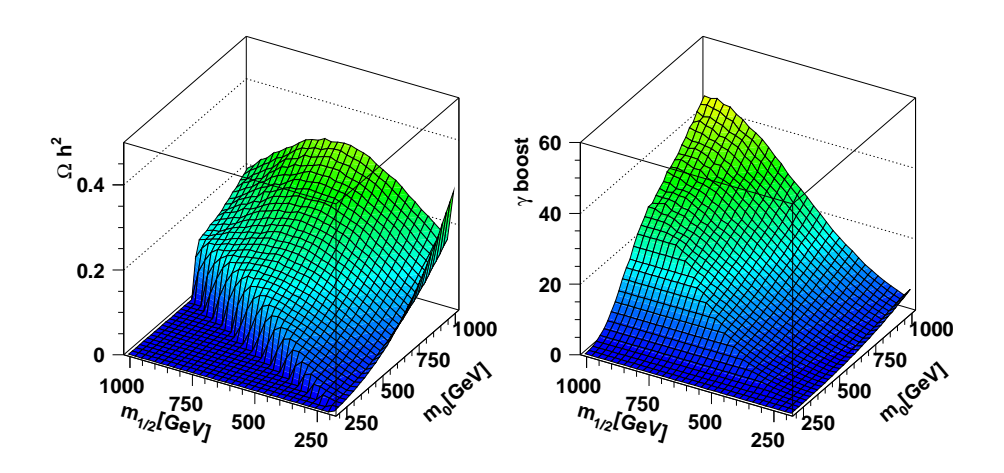


Figure 14: The relic density (left) and boost factor for the gamma rays as function of m_0 and $m_{1/2}$. Note that for large mass scales the relic density is reduced due to significant coannihilation cross sections, which are not operative in the present universe, thus causing large boost factors. For small mass scales the boost factor is practically proportional to the relic density, since both are inversely proportional to the annihilation cross section.

- The size of the galaxy is determined by a cylindrical box with half height h=4 kpc and radius r=30 kpc, as in Galprop. The solar system is at a distance of 8.5 kpc from the center. Outside this cylinder the diffusion stops and the particles escape.
- The energy dependence of the diffusion constant was taken to be the same as in Galprop and given by:

$$D = \beta D_0 \cdot (p/p_0)^{\alpha},$$

where $\beta = v/c$ is the velocity, $D_0 = 42 \cdot 10^{-27} \ cm^2/s$ is the diffusion coefficient at momentum $p_0 = 1 \ \text{GeV}$ and $\alpha = 0.33$. This diffusion coefficient is at least a factor 7 larger than the default one in DarkSusy and has a much weaker energy dependence, which is of importance mainly for antiprotons.

- The large diffusion constant implies that the galactic center starts to contribute significantly to the antiproton flux in the solar system. Therefore the effective thickness of the disk was increased from 0.1 to 0.5 kpc and the density of hydrogen in the disc was increased from 1 to 3 GeV/cm⁻³, thus increasing the interactions between antiprotons and protons in the disc. The density of hydrogen in the halo was neglected.
- The energy loss $dE/dt = \zeta E^2$ of the positrons (mainly by synchrotron radiation and inverse Compton scattering on star light) was doubled using $\zeta = 1.52 \cdot 10^{-9} \ yr^{-1} \ GeV^{-1}$, following Galprop [65] and [66].
- The Dark Matter halo profile is usually assumed to be of the Navarro, Frenk & White (NFW) type [67], as supported by numerical simulations of galaxy formation [68, 69]. Effectively we have chosen for the Dark Matter density distribution an isothermal spherical symmetric profile:

$$\rho(r) = \rho_0 \cdot \left(\frac{r}{a}\right)^{-\gamma} \left[1 + \left(\frac{r}{a}\right)^{\alpha}\right]^{\frac{\gamma - \beta}{\alpha}},$$

where a is a scale radius and the slopes α , β and γ can be thought of as the radial dependence at $r \approx a$, r >> a and r << a, respectively. At large distances we expect a $1/r^2$ dependence for a flat rotation curve, while at small distances more a 1/r dependence is needed. For definiteness we use the default $(\alpha, \beta, \gamma) = (1,3,1)$ for a scale a = 10 kpc, but e.g. (1.5,2,1) for a=2 kpc yields practically identical results. At a distance less than 10^{-5} kpc from the center the profile is kept constant to avoid any singularity. The density ρ_0 is adjusted such that the local halo density is in the range 0.2-0.8 GeV/cm³, as required by the rotation curve of our galaxy [51]. The halo density increases quite steeply towards the center, so most annihilations will take place in the center of the galaxy, thus producing there gamma rays, positrons and antiprotons. Different halo profiles are compared in Fig. 11. The percentage of gamma rays coming from the center depends on the halo profile and on the solid angle, as shown on the right hand side of Fig. 11. The positrons only reach the detector from a much smaller region due to the higher energy losses, while the antiprotons come from an intermediate region, as shown in Fig. 11 as well. These curves were obtained by calculating the flux for a halo profile truncated after a given radius.

The gamma rays can travel over large distances without loosing energy, but they will arrive at the detector only, if they were emitted along the line of sight. Antiprotons and positrons on the other hand change direction during the propagation along the magnetic field lines and by collisions, so they can arrive at the detector even if they were not emitted along the line of sight. This causes a larger acceptance for the antiprotons and positrons in comparison with the gamma rays, as shown in Fig. 12. Here the gamma flux at the Earth - n_{γ} per unit of time, surface and solid angle - from neutralino annihilation in the galactic halo can be written as:

$$\frac{dn_{\gamma}}{dt\ dS\ d\Omega} = \frac{1}{4\pi} \frac{N_{\gamma} \langle \sigma v \rangle}{m_{\chi}^2} \int_{l.o.s.} \rho_{\chi}^2 ds = \frac{1}{4\pi} \frac{N_{\gamma} \langle \sigma v \rangle}{m_{\chi}^2} \langle J \rangle, \tag{10}$$

where N_{γ} is the number of photons per annihilation (about 38 for b-quark final states) and < J > is the averaged value of the integral of the neutralino density squared along the line of sight. Since the density peaks at the center, the averaged value depends on the solid angle over which one averages. For the chosen profile < J > is about 20000 for a solid angle of 10^{-3} sr towards the center of the galaxy and 1000 for $d\Omega = 0.17$ sr, which is the solid angle used for the EGRET data.

• Diffusive reacceleration is an essential ingredient of Galprop, of special importance for the antiprotons. DarkSusy has neither the antiproton background spectrum from nuclear interactions nor the possibility of reacceleration. Therefore we used the parametrization of the antiproton spectrum from Simon, Molnar and Rösler [70]. The effect of the reacceleration is a flattening of the antiproton spectrum, which was simulated in DarkSusy by a larger value of the solar modulation constant Φ . With the parametrization from Simon et al., the large diffusion coefficient and $\Phi = 1200$ MeV we could reproduce the Galprop spectra for data from the years 1997 and 1998 sufficiently well. We will use only data from this part of the solar cycle.

The annihilation cross sections in DarkSusy differs considerably from the one in Micromegas [58] for large $\tan \beta$. This was traced back to a different width of the pseudoscalar Higgs boson. Micromegas follows the usual procedure of minimizing the Higgs potential at a scale given by $\sqrt{m_{\tilde{t}_1}m_{\tilde{t}_2}}$, which minimizes the higher order corrections. Furthermore, the pseudoscalar Higgs width is determined by the Yukawa couplings, of which the most important one in our case is the one given by m_b . However, the QCD corrections to the width lead to expressions of the type $m_b(\mu)(1+c_1\alpha_s(\mu)/\pi \ln(\mu^2/m_A^2)+...$; the large logarithms are minimized by choosing for the renormalization scale $\mu=m_A$. After using the running b-mass in DarkSusy to calculate the width, good agreement in the cross sections was found for the large $\tan \beta$ region, where pseudoscalar Higgs exchange dominates.

The relic density was calculated with Micromegas as well, since this program is particularly suited for large $\tan \beta$, where the Higgs exchange and its loop corrected width are important and it furthermore incorporates all coannihilation channels. Micromegas was interfaced to the program package Suspect, which calculates the low energy SUSY masses from the GUT scale parameters [56]. The problem of calculating the relic density at large $\tan \beta$ [71] is caused by the fact that both the pseudoscalar Higgs mass and its width have large corrections: the mass at tree level is determined by $\sqrt{m_1^2 + m_2^2}$ evaluated at the electroweak scale, but as can be seen from Fig. 1, the running of m_2^2 becomes steep at low energies. Since m_2^2 becomes negative for large $\tan \beta$, the tree level mass becomes small or even negative and a positive final mass is obtained by radiative corrections. Therefore the different calculations give quite a spread in masses [72] and depend sensitively on the scale, where the Higgs potential is minimized.

The following data were used in the fit:

- Gamma ray data from the galactic center in the angular range $330^{\circ} < \ell < 30^{\circ}$ and $-5^{\circ} < b < 5^{\circ}$ from the EGRET space telescope, which has been taking data for about 9 years on the NASA Compton Gamma Ray Observatory (CGRO). We use the data as presented in Ref. [73].
- Positron data from AMS [74] and HEAT [75].
- Antiproton data from BESS in the years 1997 and 1998 [76]

In order to see if the deficiencies in the galactic data on positron, antiprotons and gamma rays can be fitted by the contributions from neutralino annihilation, the following strategy was persued. A χ^2 minimization was performed between the combined data and the sum of the annihilation signal and background. The normalizations of the fluxes of positrons, antiprotons and gamma rays from neutralino annihilation, the so-called boost factors, were taken as free parameters in the fit for a given neutralino mass, since the annihilation rate is proportional to the Dark Matter density squared, so any clustering of dark matter can increase the absolute normalization. The normalization of the background was not varied, since it is well determined by other data, which Galprop used to fit

the diffusion parameters. The Galprop data describes well the positrons and gamma rays in the region where the neutralino annihilation does not contribute, but fails for the high energy parts of the spectra. The antiprotons are too low over the whole spectrum for the diffusion parameters determined from the B/C fraction, as mentioned in the previous section.

The χ^2 function for gamma rays was defined as $\sum_i (f_\gamma D_i - T)^2/(f_\gamma \sigma_i)^2 + (1 - f_\gamma)^2/\sigma_n^2$, where the sum runs over all data bins with errors σ_i and T is the sum of the parametrized background from nuclear interactions, as calculated by Galprop and the contribution from neutralino annihilation, as calculated by DarkSusy with the modifications mentioned above. f_γ is a common normalization factor for all data points with a systematic error given by σ_n . Normally f_γ was set to one, but sometimes it was left free in the fit in order to study the effect of possible correlations between the data points. Similar χ^2 functions were defined for the antiprotons and positrons and the total χ^2 was simply the sum of the χ^2 contributions for gamma rays, antiprotons and positrons, since no correlations exist.

The χ^2 function was minimized by the Minuit package[77] and the fit was repeated for all values of the SUSY parameters $m_0, m_{1/2}, \tan \beta$, where the mass scales were varied between 200 and 1000 GeV and $\tan \beta$ was varied between 50 and 55. The sign of the μ parameter was chosen positive, as preferred by the data on $Br(b \to X_s \gamma)$ and the anomalous magnetic moment of the muon $g_{\mu} - 2$ [59].

The boost factors for positrons, antiprotons and gamma rays are shown as function of m_0 and $m_{1/2}$ for tan β =51 in Fig. 13. They were all close to each other over most of the parameter space, which is absolutely non-trivial, if one considers the large enhancements for positrons and antiprotons from the diffusion as compared to gamma rays, as shown before in Fig. 12. This is a strong indication that the deficiencies in the prediction of the antiprotons, positrons and gamma rays are indeed due to the missing dark matter annihilation with a standard dark matter halo profile. One expects a similar boost, since the fluxes all originate from quite a large region of the galaxy, as shown before in Fig. 11, so the averaging over the clumpiness should be similar for all. The boost factors are determined by the present annihilation cross section at a temperature of a few Kelvin, while the relic density is determined by the cross section during freeze out, which is about $m_{\chi}/25$ or 10^{14} K. At the high temperatures coannihilations can become important, especially at high mass scales, so the annihilation cross sections can become large, but the boost factors can be large as well due to the small annihilation cross section in the present universe. This is demonstrated by a comparison of the relic density and the boost factor in Fig. 14, where at large m_0 and $m_{1/2}$ the relic density is small due to coannihilation, but the boost factors are large. Small boost factors are only obtained at small mass scales for which the neutralino annihilation cross sections are large (see Fig. 7).

The regions of parameter space allowed by the WMAP data are plotted in Fig. 15 for different values of $\tan \beta$. It is clear that for $\tan \beta \approx 50$ only a small region is allowed, if in addition the electroweak constraints from the Higgs mass and $b \to X_s \gamma$, and the requirement that the LSP is a neutral particle have to be fulfilled. Values of $\tan \beta$ below 50 are excluded completely, if one wants to be consistent with all constraints and if one requires in addition that the boost factors are below 10. The last requirement implies that clumpiness can enhance the annihilation signal by at most a factor of 10, which is the value suggested by simulations of galaxy formation and it excludes the regions of coannihilations between staus and neutralinos. The boost factors are strongly correlated with the value of the local halo density ρ_{χ} . To obtain a conservative excluded region by the requirement that the boost factor is below 10, ρ_{χ} was set to its maximum allowed value of 0.2-0.8 GeV/cm³. Coannihilations occur if the staus are nearly degenerate in mass with the neutralinos, which happens next to the region labelled "excl. LSP" in fig. 15. In this region the stau is the Lightest Supersymmetric Particle (LSP) and next to it the stau is almost degenerate with the neutralino, so it cannot decay into a neutralino and tau. In this case the stau is practically stable and can annihilate with a neutralino into a tau plus photon. This coannihilation reduces the relic density to values required by the WMAP data. For values of $\tan \beta$ above 50 there are quite a range of neutralino masses allowed, since for larger values of $\tan \beta$ one hits the resonance of pseudoscalar Higgs exchange, in which case much heavier neutralinos are allowed, as shown in Fig. 15 (bottom left).

The results of two good fits with two different neutralino masses (207 and 427 GeV) are shown in Figs. 16, 17 and 18. The parameters are summarized in Table 1. Fig. 15 shows that these

parameters are close to masses at the lower and upper range of possible masses. As indicated in the figures the boost factors for antiprotons, positrons and gamma rays are all similar for the NRW halo profile discussed before and the χ^2 improves significantly with the inclusion of Dark Matter in the fits. The $\chi^2/d.o.f.$ is reduced from 110/38 for the "background-only" fit to 34/35 for the fit including neutralino annihilation. This corresponds to an increase in probability from about 10^{-8} to 0.5, as shown in Table 2 together with the results for the individual spectra. For the antiprotons the increase in probability is the least significant, as expected, since the shape of background and signal are similar. This causes also a strong correlation between the normalization of the data and the boost factor. For the gamma rays and positrons this correlation is less severe because of the different shapes of signal and background. Leaving all the normalizations free in the fit does not change the results significantly for normalization errors below 10 %, since mainly the antiprotons are affected, but they anyhow do not have a strong statistical significance. They are nevertheless important for the analysis, since they check the expectation of similar boost factors for all species and constrain the analysis by the requirement of not overproducing the antiprotons.

It is interesting to see what are the prospects to observe the neutralinos in other channels or by direct detection for the points of parameter space selected by the present analysis. For a neutralino mass of 207(427) GeV the flux of muons with energy above 1 GeV from neutralino annihilation inside the sun are only 8 (0.3) $km^{-2} yr^{-1}$, while the flux from the earth is even smaller for the SUSY and halo parameters considered in this analysis. These fluxes were calculated with DarkSusy [55].

The cross section for *direct* Dark Matter detection was calculated with DarkSusy [55] as well. For the heavier masses the cross section rapidly decreases, but the projected sensitivity of future direct detection experiments may be sufficient, if the neutralino mass happens to be at the lower range allowed by the present analysis, as demonstrated in Fig. 19.

Unfortunately, the high cross section deduced from the 6.3σ solar modulation signal observed in the DAMA experiment [78] seems difficult to reconcile with the present analysis, since the diagrams for neutralino-nucleon scattering are by crossing symmetry similar to the ones for neutralino annihilation, so such a large cross section in direct detection would produce an excessive amount of positrons, antiprotons and gamma rays.

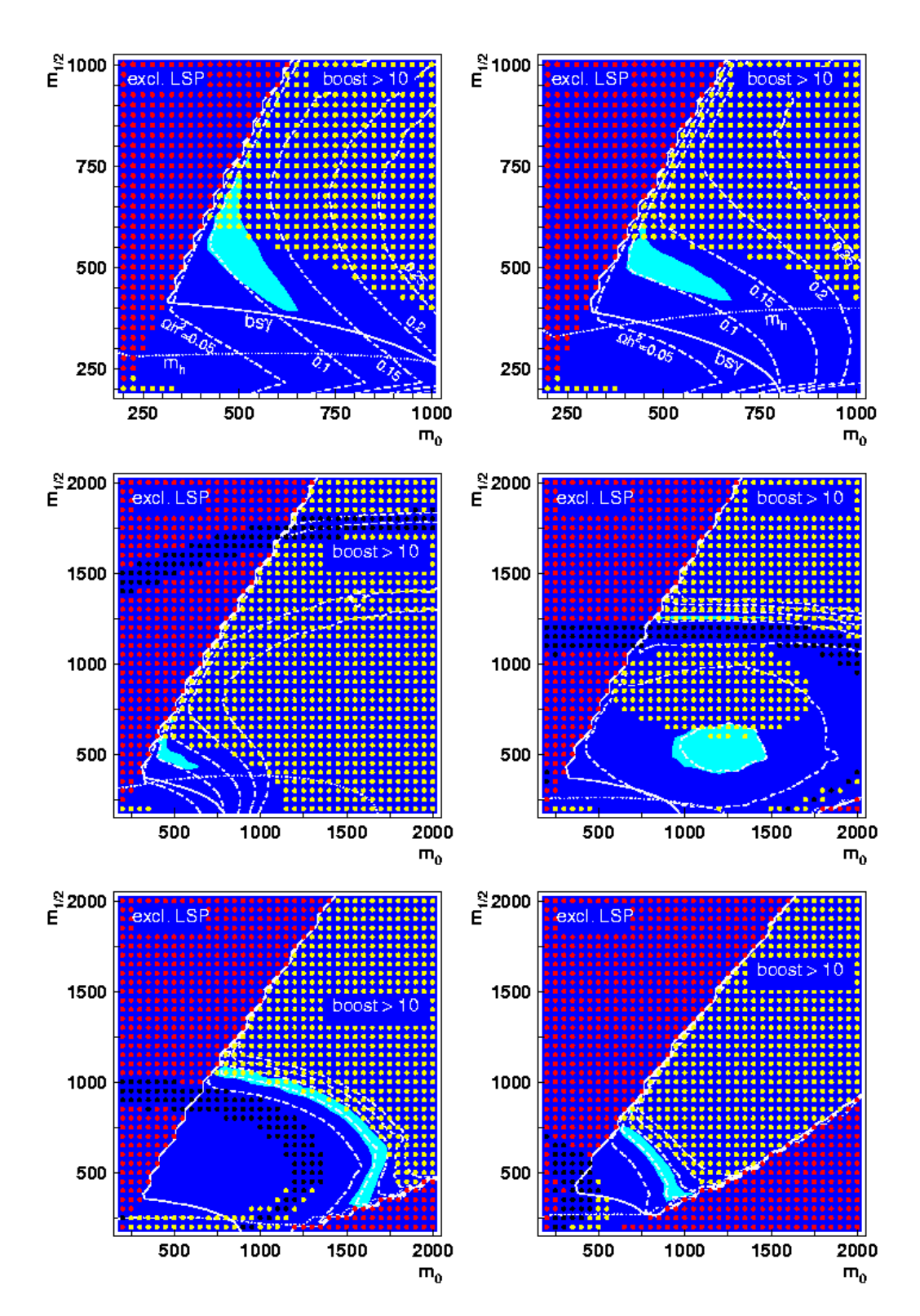


Figure 15: The region of relic density allowed by the WMAP data. The upper row is for $\tan \beta = 51$ and $A_0 = 0$ (left) and $A_0 = m_0$ (right), which shows that the role of Higgs constraint (dotted line) and $b \to X_s \gamma$ constraint (solid line) are interchanged for the different values of the trilinear coupling, but the lower limit on $m_{1/2}$ is not very sensitive to A_0 . The light shaded (blue) area is the region allowed by WMAP and the contours of larger Ωh^2 are indicated by the dashed lines in steps of 0.05. The second (third) row show the same information for a larger region for $\tan \beta = 51$, 52 (l. and r.) (53 and 55 (l. and r.)). The excluded regions, where the stau would be the LSP or EWSB fails or the boost factors are above 10 are indicated by the dots. The black dots indicate the resonance region, where $|m_A - 2m_{\chi_0}| \leq 10$ GeV. For $\tan \beta > 52$ the acceptable values for the relic densities are for $m_{1/2}$ values above the resonance region.

Parameter	Value	Value	
m_0	$500 \mathrm{GeV}$	$1000 \mathrm{GeV}$	
$m_{1/2}$	$500 \mathrm{GeV}$	$1000 \mathrm{GeV}$	
A_0	$500 \mathrm{GeV}$	$0~{ m GeV}$	
$\tan eta$	51	53	
$\operatorname{sgn}\mu$	+	+	
Particle	Mass [GeV]	Mass [GeV]	
$\chi^{0}_{0,1,2,3}$	207,375,568,583	427, 783, 1119, 1127	
$N_{0,1,2,3}^{\chi^0} \ N_{0,1,2,3}^{\chi^0} \ \chi_{0,1}^{\pm} \ ilde{g} \ ilde{t}_{1,2} \ ilde{b}_{1,2}$	0.995, 0.017, 0.093, 0.036	$0.999,\ 0.004,\ 0.047,\ 0.019$	
$\chi_{0.1}^{\pm}$	375, 584	783, 1128	
$\widetilde{\widetilde{g}}$	1121	2154	
$ ilde{t}_{1,2}$	852, 1010	1616, 1842	
$ ilde{b}_{1,2}$	909, 998	$1719,\ 1831$	
$ ilde{ au}_{1,2}$	292, 535	591, 1037	
h,H	116, 504	121,823	
A,H^\pm	506, 515	832, 838	
Observable	Value	Value	
$Br(b \to X_s \gamma)$ [58]	$2.73 \cdot 10^{-4}$	$3.45 \cdot 10^{-4}$	
$a_{\mu} \ [58]$	$258 \cdot 10^{-11}$	$67 \cdot 10^{-11}$	
Ωh^2 [58]	0.114	0.095	
$<\sigma v(\chi + \chi \rightarrow anything)>$	$1.6 \cdot 10^{-26} cm^3/s$	$4.5 \cdot 10^{-26} cm^3/s$	
$<\sigma v(\chi+\chi\to b\overline{b})>$	$1.4 \cdot 10^{-26} cm^3/s$	$4.0 \cdot 10^{-26} cm^3/s$	
$<\sigma v(\chi+\chi\to \tau\overline{\tau})>$	$0.2 \cdot 10^{-26} cm^3/s$	$0.5 \cdot 10^{-26} cm^3/s$	

Table 1: mSUGRA parameters with the corresponding supersymmetric particle spectrum and some predicted observables for an LSP mass of 207 and 427 GeV. The cross sections were calculated by DarkSusy [55], which agree with the cross sections from Micromegas [58] for these parameters after the modifications to DarkSusy mentioned in the text. The particle spectrum was calculated by Suspect [56] and Feynhiggsfast [57].

	Background		$m_{\chi} = 207 \text{ GeV}$		$m_{\chi} = 427 \text{ GeV}$	
	$\chi_b^2/d.o.f.$	Prob.	$\chi^2_{b+s}/d.o.f.$	Prob.	$\chi^2_{b+s}/d.o.f.$	Prob.
Positrons	59.4/18	$2.5 \cdot 10^{-6}$	16.7/17	0.48	14.3/17	0.59
Antiprotons	15.9/13	$2.6 \cdot 10^{-1}$	6.6/12	0.89	6.7/12	0.88
Gammas	34.5/7	$1.4 \cdot 10^{-5}$	9.5/6	0.15	12.3/6	0.06
Total	110/38	$6.7 \cdot 10^{-9}$	33.7/35	0.53	33.3/35	0.55

Table 2: The χ^2 and probabilities of the fits for fluxes from background only, i.e. from nuclear interactions (labelled "b") and for fluxes including "signal" contributions from neutralino annihilation (labelled "b+s") for two neutralino masses.

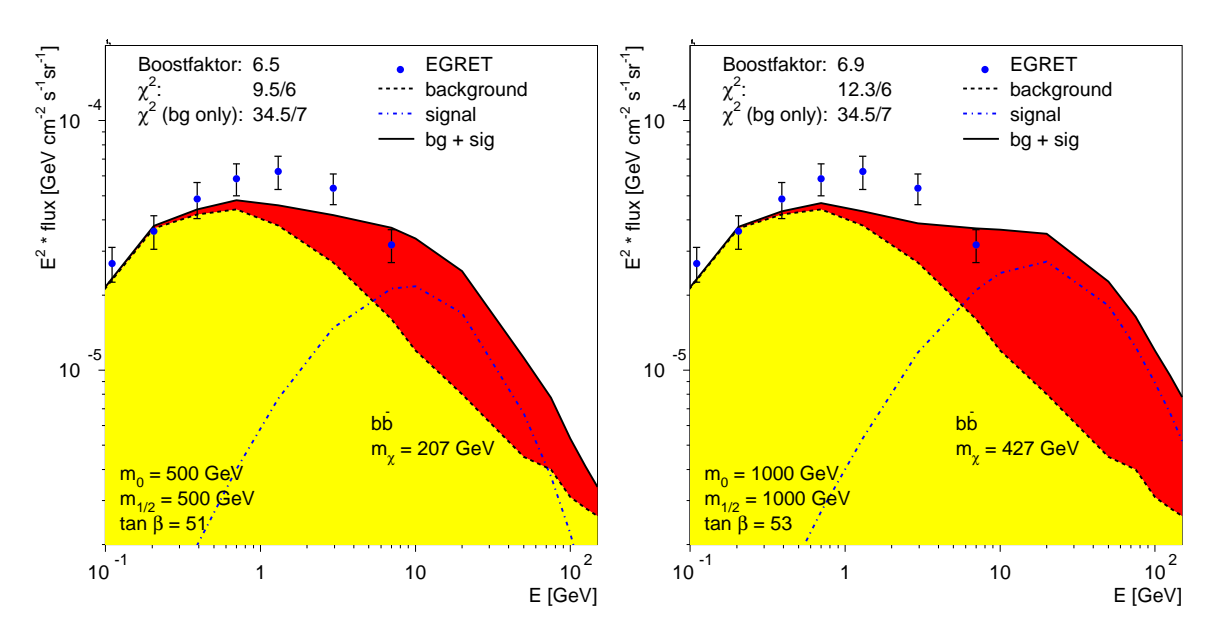


Figure 16: Gamma ray spectrum with contributions from nuclear interactions (grey/yellow) and neutralino annihilation (dark/red) for a neutralino mass of 207 (left) and 427 GeV (right).

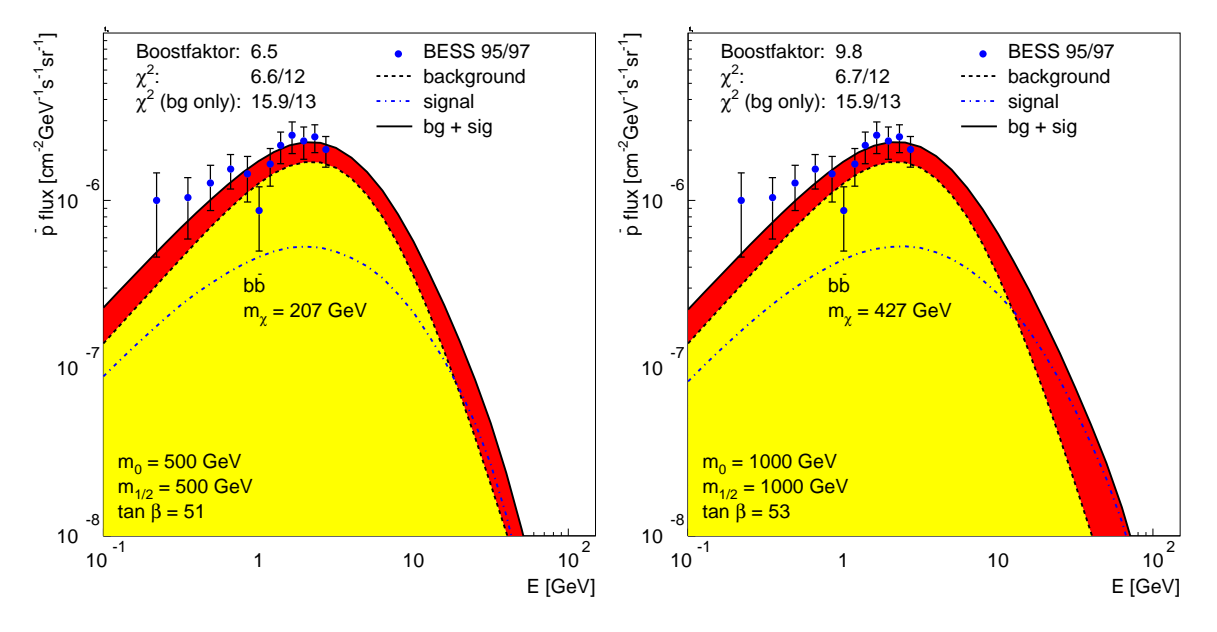


Figure 17: Antiproton spectrum with contributions from nuclear interactions (grey/yellow) and neutralino annihilation (dark/red) for a neutralino mass of 207 (left) and 427 GeV (right).

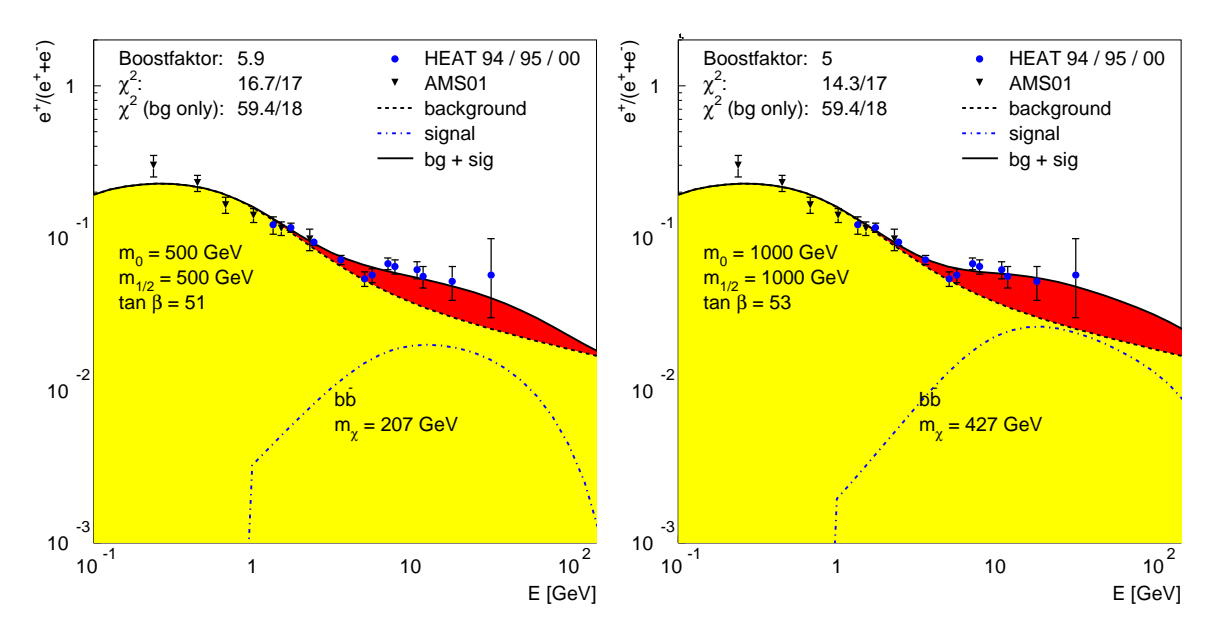


Figure 18: Positron spectrum with contributions from nuclear interactions (grey/yellow) and neutralino annihilation (dark/red) for a neutralino mass of 207 (left) and 427 GeV (right).

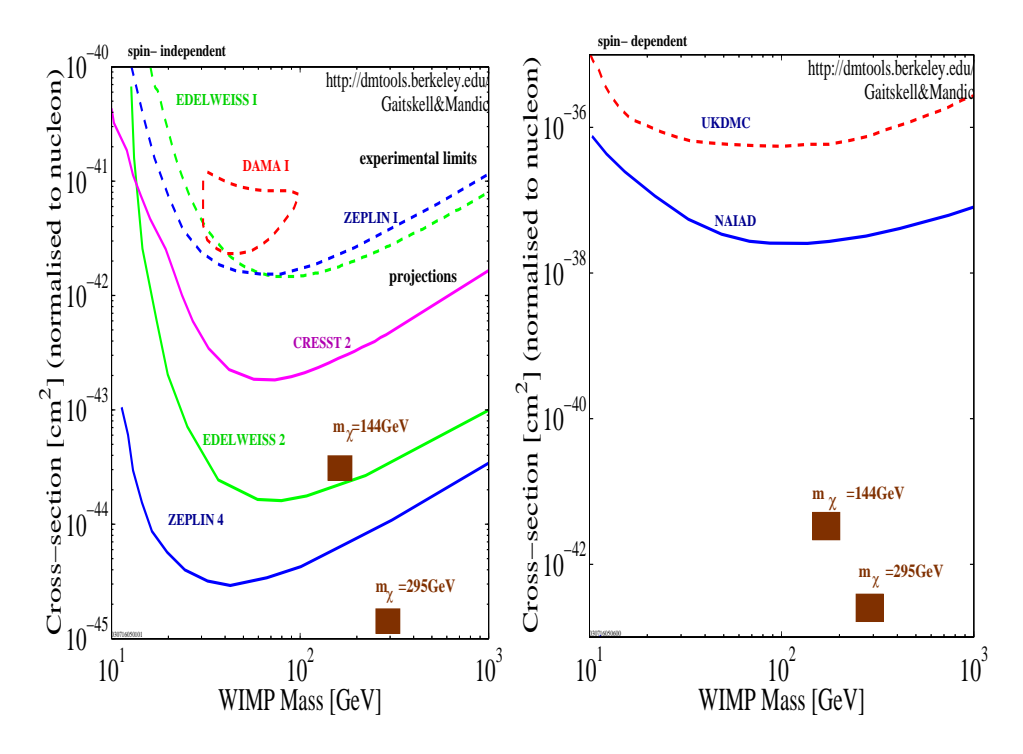


Figure 19: The spin independent (left) and spin dependent (right) cross section for direct WIMP detection on protons in comparison with existing (dashed lines) and projected (solid lines) limits and the cross section expected for neutralino masses of 144 and 295 GeV (squares). A neutralino mass as low as 144 GeV is at the border of compatibility with the constraints from the Higgs mass and $b \to X_s \gamma$, so a mass between the two masses indicated is more likely.

6 Conclusion

The galactic models can very well describe the nuclear reactions, especially the ratio of secondary to primary produced nuclei and the small concentration of long-lived radioactive nuclei. These observations fix the diffusion parameters, especially the need for diffusive reacceleration as an additional term in the diffusion equation was emphasized by Moskalenko and Strong. However, the diffusion parameters from such a global view produce too few antiprotons, too few hard gammas and to a lesser extent to few hard positrons. Up to now many investigations on the fluxes of positrons, antiprotons and gamma rays have been performed, either to study the contributions from neutralino annihilation or to study "Local Bubble" type contributions to defeat the deficiencies of the standard propagation models. However, it is shown that Dark Matter annihilation within the Constrained Minimal Supersymmetric Model can solve these deficiencies simultaneously.

This is the first time that these fluxes are studied in a global fit using the best available diffusion parameters without artificial constructs to remedy the deficiencies of the galactic models and add to the contributions from nuclear interactions the ones from neutralino annihilation in the Constrained Minimal Supersymmetric Model (CMSSM) with all the known constraints from electroweak precision data and the relic density from the WMAP satellite. Actually, all we need from the supersymmetric model to fill up the deficiencies is a neutralino with a thermally averaged annihilation cross section times relative neutralino velocities of about 10^{-26} cm³/s for the present universe, i.e. without coannihilation. This cross section can be smaller, if the halo distribution of the neutralinos is not smooth, but clumpy, thus enhancing the annihilation rate by a certain "boost factor", which simulations of galaxy formation show to be of "the order of a few". The boost factors for antiprotons, positrons and gamma rays were left as independent free parameters in the fit, but they all come out to be similar for a given halo profile and given neutralino mass. This result is non-trivial given the very different mean free paths of positrons, antiprotons and gamma rays and provides a strong support for neutralino annihilation as a common origin of the deficiencies. The needed large cross sections are obtained in the CMSSM only for relatively light neutralinos in the mass range of 150 - 400 GeV and $\tan \beta > 50$. At large $\tan \beta$ the annihilation is dominated by pseudoscalar Higgs exchange into bb quark pairs. The upper neutralino mass is limited by the rather arbitrary requirement that the boost factors are below 10 and the lower mass limit is given by the electroweak constraints at large tan β . The probability of the global fit to galactic fluxes of positrons, antiprotons and gamma rays increases from 10⁻⁸ to 0.5 by including the contribution from neutralino annihilation, which can be interpreted in case of gaussian errors as an improvement by about 6 standard deviations. These facts, statistical significance of the global fit combined with similar boost factors for positrons, antiprotons and gamma rays, provide strong experimental evidence for the supersymmetric nature of Dark Matter.

7 Acknowledgements

We thank V. Moskalenko and A. Strong for sharing with us all their knowledge about our galaxy, O. Reimers to provide us with the EGRET data, L.Bergström, J. Edsjö and P. Ullio for useful discussions about DarkSusy and neutralino annihilation, F. Stoehr, V. Springel and G. Börner for discussions on haloes, A. Belyaev and G. Bélanger for discussions about relic density, A. Pukhov for discussions about CalcHEP, J. Kühn for a discussion on radiative corrections to the Higgs boson widths, and last but not least D. Kazakov and his group for early contributions to this analysis.

This work was supported by the DLR (Deutsches Zentrum für Luft- und Raumfahrt) and the BMBF (Bundesministerium für Bildung und Forschung).

References

- [1] The results of the first year of operation of the WMAP satellite can be found on the Web: http://map.gsfc.nasa.gov/m_mm/pub_papers/firstyear.html
- [2] C.L. Bennett, et al., astro-ph/0302207.

- [3] D.N. Spergel, et al., astro-ph/0302209.
- [4] L. Verde et al., astro-ph/0302218
- [5] J. Ellis et al., Nucl. Phys. **B238** (1984) 453.
- [6] G. Jungman, M. Kamionkowski and K. Griest, Phys. Rep. **267** (1996) 195.
- [7] I.V. Moskalenko, A.W. Strong, J.F. Ormes and M.S. Potgieter, Astrophys. J. 565 (2002) 280.
- [8] A.W. Strong, I.V. Moskalenko and O. Reimer, Astrophys. J. 537 (2000) 763.
- [9] A.W. Strong, I.V. Moskalenko, S.G. Mashnik and J.F. Ormes, Astrophys. J. 586 (2003) 1050.
- [10] L. Bergstrom, Rept. Prog. Phys. **63** (2000) 793 [arXiv:hep-ph/0002126];
- [11] S. Rudaz and F. W. Stecker, Astrophys. J. **325** (1988) 16.
- [12] G. Chardin, DAPNIA-02-413 Prepared for 37th Rencontres de Moriond on the Cosmological Model, Les Arcs, France, 16-23 Mar 2002
- [13] J. Orloff, E. Nezri and V. Bertin, arXiv:hep-ph/0301215.
- [14] E. Nezri, arXiv:hep-ph/0211082.
- [15] V. Bertin, E. Nezri and J. Orloff, Eur. Phys. J. C 26 (2002) 111 [arXiv:hep-ph/0204135].
- [16] V. D. Barger, F. Halzen, D. Hooper and C. Kao, Phys. Rev. D **65** (2002) 075022 [arXiv:hep-ph/0105182].
- [17] J. L. Feng, K. T. Matchev and F. Wilczek, Phys. Rev. D **63** (2001) 045024 [arXiv:astro-ph/0008115].
- [18] F. Halzen, arXiv:astro-ph/9508020.
- [19] M. Kamionkowski, K. Griest, G. Jungman and B. Sadoulet, Phys. Rev. Lett. 74 (1995) 5174 [arXiv:hep-ph/9412213].
- [20] A. Morselli, Int. J. Mod. Phys. A 17 (2002) 1829.
- [21] F. Donato, N. Fornengo, D. Maurin, P. Salati and R. Taillet, arXiv:astro-ph/0306207.
- [22] J. Edsjo, arXiv:astro-ph/0211354.
- [23] A. Birkedal-Hansen and B. D. Nelson, Phys. Rev. D 67 (2003) 095006 [arXiv:hep-ph/0211071].
- [24] V. Bertin, E. Nezri and J. Orloff, JHEP **0302** (2003) 046 [arXiv:hep-ph/0210034].
- [25] E. A. Baltz, J. Edsjo, K. Freese and P. Gondolo, Phys. Rev. D 65 (2002) 063511 [arXiv:astro-ph/0109318].
- [26] A. B. Lahanas and V. C. Spanos, Eur. Phys. J. C 23 (2002) 185 [arXiv:hep-ph/0106345].
- [27] T. Nihei, L. Roszkowski and R. Ruiz de Austri, JHEP **0105** (2001) 063 [arXiv:hep-ph/0102308].
- [28] L. Bergstrom, J. Edsjo and C. Gunnarsson, Phys. Rev. D **63** (2001) 083515 [arXiv:astro-ph/0012346].
- [29] P. Ullio, L. Bergstrom, J. Edsjo and C. Lacey, Phys. Rev. D 66 (2002) 123502 [arXiv:astro-ph/0207125].
- [30] A. Cesarini, F. Fucito, A. Lionetto, A. Morselli and P. Ullio, arXiv:astro-ph/0305075.

- [31] P. Ullio, Int. J. Mod. Phys. A 17 (2002) 1777.
- [32] E. A. Baltz, J. Edsjo, K. Freese and P. Gondolo, arXiv:astro-ph/0211239.
- [33] J. R. Ellis, arXiv:astro-ph/0305038;
- [34] arXiv:astro-ph/0304183.
- [35] J. R. Ellis, J. L. Feng, A. Ferstl, K. T. Matchev and K. A. Olive, Eur. Phys. J. C 24 (2002) 311 [arXiv:astro-ph/0110225].
- [36] G. L. Kane, L. T. Wang and T. T. Wang, Phys. Lett. B 536 (2002) 263 [arXiv:hep-ph/0202156].
- [37] E. W. Kolb and M. S. Turner, "The Early Universe," Frontiers in Physics, Addison-Wesley, 1990.
- [38] C. Calcaneo-Roldan and B. Moore, Phys. Rev. D 62 (2000) 123005 [arXiv:astro-ph/0010056].
- [39] P. Gondolo, Phys. Lett. B **494** (2000) 181 [arXiv:hep-ph/0002226].
- [40] E. A. Baltz, C. Briot, P. Salati, R. Taillet and J. Silk, Phys. Rev. D 61 (2000) 023514 [arXiv:astro-ph/9909112].
- [41] A. Corsetti and P. Nath, Int. J. Mod. Phys. A 15 (2000) 905 [arXiv:hep-ph/9904497].
- [42] L. Bergstrom, J. Edsjo, P. Gondolo and P. Ullio, Phys. Rev. D 59 (1999) 043506 [arXiv:astro-ph/9806072].
- [43] A. Bottino, F. Donato, N. Fornengo and P. Salati, Phys. Rev. D 58 (1998) 123503 [arXiv:astro-ph/9804137].
- [44] P. Ullio and L. Bergstrom, Phys. Rev. D 57 (1998) 1962 [arXiv:hep-ph/9707333].
- [45] Z. Bern, P. Gondolo and M. Perelstein, Phys. Lett. B 411 (1997) 86 [arXiv:hep-ph/9706538].
- [46] L. Bergstrom, J. Edsjo and P. Gondolo, Phys. Rev. D 55 (1997) 1765 [arXiv:hep-ph/9607237].
- [47] G. Jungman and M. Kamionkowski, Phys. Rev. D 51 (1995) 3121 [arXiv:hep-ph/9501365].
- [48] A. Bottino, N. Fornengo, G. Mignola and L. Moscoso, Astropart. Phys. 3 (1995) 65 [arXiv:hep-ph/9408391].
- [49] G. Jungman and M. Kamionkowski, Phys. Rev. D 49 (1994) 2316 [arXiv:astro-ph/9310032].
- [50] A. Bottino, V. de Alfaro, N. Fornengo, A. Morales, J. Puimedon and S. Scopel, Mod. Phys. Lett. A 7 (1992) 733.
- [51] L. Bergstrom, P. Ullio and J. H. Buckley, Astropart. Phys. 9 (1998) 137 [arXiv:astro-ph/9712318].
- [52] Reviews and original references can be found in: W. de Boer, Prog. Part. Nucl. Phys. **33** (1994) 201 [arXiv:hep-ph/9402266];
 - A.B. Lahanus and D.V. Nanopoulos, Phys. Rep. 145 (1987) 1;
 - H.E. Haber and G.L. Kane, Phys. Rep. **117** (1985) 75;
 - M.F. Sohnius, Phys. Rep. **128** (1985) 39;
 - H.P. Nilles, Phys. Rep. **110** (1984) 1;
 - P. Fayet and S. Ferrara, Phys. Rep. **32** (1977) 249.
- [53] A.W. Strong and I.V. Moskalenko, Astrophys. J. **509** (1998) 212.
- [54] I.V. Moskalenko and A.W. Strong, Astrophys. J. **493** (1998) 694.

- [55] DarkSUSY, P. Gondolo, J. Edsjo, L. Bergstrom, P. Ullio and E. A. Baltz, arXiv:astro-ph/0012234 and http://www.physto.se/edsjo/darksusy/.
- [56] A. Djouadi, J. L. Kneur and G. Moultaka, arXiv:hep-ph/0211331.
- [57] S. Heinemeyer, W. Hollik and G. Weiglein, arXiv:hep-ph/0002213.
- [58] G. Bélanger, F. Boudjema, A. Pukhov and A. Semenov, arXiv:hep-ph/0210327 and http://wwwlap.in2p3.fr/lapth/micromegas.
- [59] W. de Boer and C. Sander, arXiv:hep-ph/0307049 and references therein.
- [60] H. Goldberg, Phys. Rev. lett. **50** (1983) 1419.
- [61] A. Pukhov et al., arXiv:hep-ph/9908288.
- [62] K. Griest and D. Seckel, Phys. Rev. **D43** (1991) 3191
- [63] L.J. Gleeson and W.I. Axford, ApJ 149 (1967) L115; ApJ 154 (1968) 1011.
- [64] D. Casadei and V. Bindi, astro-ph/0302307.
- [65] I. V. Moskalenko and A. W. Strong, Phys. Rev. D 60 (1999) 063003 [arXiv:astro-ph/9905283].
- [66] M. Kamionkowski and M.S. Turner, Phys. Rev. D 43 (1991) 1774.
- [67] J.F. Navarro, C.S. Frank and S.D.M. WHite, ApJ 490 (1997) 493.
- [68] F. Stoehr, S. D. White, V. Springel, G. Tormen and N. Yoshida, arXiv:astro-ph/0307026;
- [69] D. Zhao, H. Mo, Y. Jing and G. Boerner, Mon. Not. Roy. Astron. Soc. 339 (2003) 12 [arXiv:astro-ph/0204108].
- [70] M. Simon, A. Molnar and S. Rösler, ApJ **499** (1998) 250; Numerical details of the background parametrization can be found in M. Horn, Diplomarbeit IEKP-KA/2002-17, http://www-ekp.physik.uni-karlsruhe.de/theses/dipl/2002.html, p. 69.
- [71] H. Baer, C. Balazs and A. Belyaev, JHEP **0203** (2002) 042 [arXiv:hep-ph/0202076].
- [72] B. Allanach, S. Kraml, and W. Porod, [arXiv:hep-ph/0207314].
- [73] A. W. Strong, I. V. Moskalenko and O. Reimer, arXiv:astro-ph/0306345.
- [74] J. Alcaraz et al. [AMS Collaboration], Phys. Lett. B 484 (2000) 10 [Erratum-ibid. B 495 (2000) 440].
- [75] S. W. Barwick et al. [HEAT Collaboration], Astrophys. J. 482 (1997) L191 [arXiv:astro-ph/9703192].
 M. A. DuVernois et al., Astrophys. J. 559 (2001) 296.
- [76] BESS Coll. S. Orito et al., Phys. Rev. Lett 84 (2000) 1078. T. Maeno et al., Atrop. Phys. 16 (2001) 121; astro-ph/0010381.
- [77] F. James, M. Roos, MINUIT Function Minimization and Error Analysis, CERN Program Library Long Writeup D506; Release 92.1, March 1992;
- [78] R. Bernabei et al., Riv. Nuovo Cim. 26 (2003) 1 [arXiv:astro-ph/0307403].